Eur. Phys. J. C (2023) 83:396
https://doi.org/10.1140/epjc/s10052-023-11516-9

THE EUROPEAN PHYSICAL JOURNAL C

Regular Article - Experimental Physics

New limit on ^{94}Zr double beta decay to the 1st excited state of ^{94}Mo

E. Celi[1,2], M. Ješkovský[3], M. Laubenstein[2], S. S. Nagorny[4,5,a], V. V. Nahorna[6], S. Nisi[2], L. Pagnanini[1,2,4], P. Povinec[3], P. Wang[5,6]

[1] Gran Sasso Science Institute, 67100 L'Aquila, Italy
[2] INFN-Laboratori Nazionali del Gran Sasso, 67100 Assergi, L'Aquila, Italy
[3] Faculty of Mathematics, Physics and Informatics, Comenius University, 84248 Bratislava, Slovakia
[4] Department of Physics, Engineering Physics and Astronomy, Queen's University, Kingston, ON K7L 3N6, Canada
[5] Arthur B. McDonald Canadian Astroparticle Physics Research Institute, Kingston, ON K7L 3N6, Canada
[6] Department of Chemistry, Queen's University, Kingston, ON K7L 3N6, Canada

Received: 1 February 2023 / Accepted: 17 April 2023

Abstract A new study of double beta decay processes in natural Zr isotopes using Zr metal samples and an ultra-low-background high-purity germanium detectors was performed at Laboratori Nazionali del Gran Sasso of INFN (Italy). Two data sets were collected with a 736.35 g and a 129.94 g Zr metal over 59.7 days and 37.3 days, respectively, and were used for a detailed analysis. A new limit on the double beta decay of ^{94}Zr to the 1st excited level of ^{94}Mo was set as $T^{\beta\beta}_{1/2} > 2.1 \times 10^{20}$ year, which is a factor of three better than the previous result. It is shown that the current radiopurity of Zr metal (tens of Bq/kg), produced via two methods, do not comply with the radiopurity requirements for low-background experiments. Hence, we propose to use a purified $ZrCl_4$ powder in an optimized geometry as a new approach for future experiments with extended sensitivity focused on studies of rare nuclear processes in Zr isotopes.

1 Introduction

Among the most challenging questions that are intriguing the astroparticle physics community, the Dirac vs. Majorana nature of the neutrinos is one of the most interesting, given its impact on the fundamental knowledge of the Universe [1]. The most sensitive physics process currently known to reveal the neutrino nature is the neutrinoless double beta decay of atomic nuclei (0νDBD). This is a second-order weak transition in which two neutrons simultaneously decay exchanging a virtual Majorana neutrino, so that the final state includes only two electrons and the nucleus (with the proton number changing by 2 units):

$$(A, Z) \rightarrow (A, Z+2) + 2e^{-}. \quad (1)$$

The standard model allowed counterpart of 0νDBD is two-neutrino double beta decay (2νDBD), in which two $\bar{\nu}_e$ are emitted in the final state:

$$(A, Z) \rightarrow (A, Z+2) + 2e^{-} + 2\bar{\nu}_e. \quad (2)$$

Such decays can proceed both between the ground-states (g.s.) of the initial and final nuclei, or through excited levels (exc.l.) of the daughter nuclide, if kinetically allowed and not forbidden by selection rules (momentum and parity). In the latter case, being some fraction of the decay energy emitted as γ-quanta, the remaining energy released through DBD is correspondingly lower, leading to a significant reduction of the phase space ($\propto Q^5_{\beta\beta}$), and thus increasing the expected half-life of the DBD process.

Modern experimental efforts in the field of 0νDBD studies are focused on few DBD-active isotopes – ^{76}Ge, ^{82}Se, ^{100}Mo, ^{116}Cd, ^{130}Te, ^{136}Xe – because of well-developed detector techniques (such as scintillators [2,3], semiconductor detectors [4,5], bolometers [6], scintillating bolometers [7–9], and time-projection chambers [10,11]), and due to adopting detector materials with tailored characteristics, in which the isotope of interest is present with a high mass fraction.

However, the term "well-developed detector techniques" typically consists of the combination of a few factors: (a) scientifically attractive DBD isotopes and processes to be studied; (b) the existence of an appropriate enrichment technology to significantly increase the number of decaying nuclei; (c) the existence of an appropriate detector technology; (d) the existence of appropriate detector materials in which the element of interest could be embedded in a high mass frac-

[a] e-mail: sn65@queensu.ca (corresponding author)

Published online: 11 May 2023

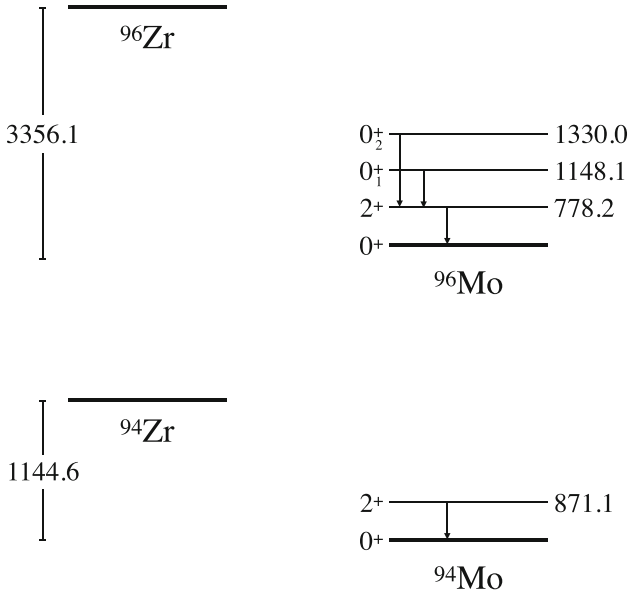

Fig. 1 First excited states of ^{96}Mo and ^{94}Mo following double beta decay of ^{96}Zr and ^{94}Zr, respectively. The reported values are in keV

tion; (e) high-quality and well-developed production technology of those detector materials; (f) market availability of the same material at the same quality grade; the last leads to additional two factors that, nevertheless, are not of minor importance (g) sufficient funding; and (h) an adequate number of research groups that would work on that topic for the period of time necessary to produce a competitive result. All previously mentioned DBD-active isotopes satisfy the above-listed criteria.

Nevertheless, several other DBD-active isotopes are considered attractive from a scientific point of view but are disfavoured due to the lack of appropriate detector technology. Among those isotopes are ^{94}Zr and ^{96}Zr [12,13]. In particular, ^{96}Zr is promising because of its high energy transition ($Q_{\beta\beta}$ = 3356.097(86) keV [14]) that naturally eliminates the background contribution to the region of interest (ROI) caused by environmental γ-radioactivity of ^{208}Tl (up to 2.6 MeV) or internal β-activity of ^{214}Bi (up to 3.27 MeV), and hence significantly reducing requirements for the detector material radiopurity. ^{96}Zr is also one of the most suitable candidates to study the DBD transitions through the exc.l. of the daughter nuclide, since the released energy with two electrons is equal to 2208 keV, when the first 0^+_1 excited level is considered, see decay scheme in Fig. 1.

On the other hand, ^{94}Zr, despite its low decay energy ($Q_{\beta\beta}$ = 1144.56 (31) keV [15]), is attractive due to its high natural isotopic abundance (17.4%) and the presence of a relatively low-energy excited level (871 keV, 2^+_1) that makes it possible to search for DBD processes to the excited level of the daughter nuclide with natural Zr metal samples and low-background HPGe detectors (see Fig. 1 and Table 1). The best current limit is rather modest, just about 5×10^{19} years, but it could be improved with a kg-scale Zr sample with high radiopurity.

Table 1 List of zirconium isotopes for which DBD to the 1st excited state is expected. We report isotopic abundance, decay modes and current best half-life limits

Isotope	Abundance (%)	Decay mode	Current limit, yr	Refs.
^{94}Zr	17.38	$\beta\beta$	5.2×10^{19}	[16]
^{96}Zr	2.8	$\beta\beta$	3.1×10^{20}	[17]

Experiments based on the calorimetric approach ("source = detector") are optimal to search for g.s.–g.s. transition, having a high electron containment efficiency, at the level of 80%. On the other hand, transitions to exc.l. require a different approach in which de-excitation γ-quanta should be effectively registered by a large volume sensitive detector with an optimized signal-to-background ratio. This is often realized by performing such measurements deep underground to reduce the cosmic-ray induced background, using well-shielded low-background HPGe gamma-spectrometers that have an excellent energy resolution. Furthermore, the sample has to be of high radiopurity, containing the isotope of interest in a high mass fraction and in an optimized geometry.

In this kind of experiments, the sensitivity scales like $T_{1/2} \propto \varepsilon \cdot \sqrt{B}$, therefore increasing the detection efficiency (ε) by optimising the sample geometry and minimizing the self-absorption of the emitted photons within the sample can be more effective than reducing the background (B) [18]. It is clear that an important increase in efficiency could lead to a higher $T_{1/2}$ sensitivity even in the presence of a larger background.

In this article, we study the radiopurity of Zr metal and Zr-containing samples, the purification methods, in order to find the optimal path to maximize the signal-to-background ratio in future experiments. Moreover, we derive new limits on DBD processes in the natural ^{94}Zr isotope as well.

In Sect. 2, we introduce Zr metal samples provided by two independent suppliers and produced using different techniques. The effectiveness of these production procedures is discussed in Sect. 3, where the results of Zr metal sample measurements are presented. In Sect. 4, we report the best half-life limit on DBD of ^{94}Zr to the exc.l. of ^{94}Mo derived from the analysis of the combined data of the two Zr metal samples. Finally, in Sect. 5, we discuss possible further steps and perspectives using a Zr-containing compound ($ZrCl_4$) adopting new purification methods.

2 Metallic zirconium production

Zirconium metal is a widely used material in chemistry, aerospace and nuclear energy industry. Zirconium, having

a low cross-section of thermal neutron capture, a relatively high melting point, a high radiation and corrosion resistivity, is one of the basic metals used in alloys for nuclear fuel elements. It is also widely used in the chemistry industry for equipment and labware utilized in a strongly acidic environment, since its corrosive resistivity is higher than that of stainless steel. Moreover, zirconium is used as a dopant in the production of dedicated alloys with a high melting point for unique and specific applications.

The nuclear power industry is the field that requires the highest chemical purity of zirconium metal, however, its production is very complex consisting of more than 25 steps [19], which can be grouped into five stages: (1) decomposition of Zr-containing ores; (2) production of ($ZrCl_4 + HfCl_4$) concentrate with high Hf-content (up to 3%); (3) separation of $ZrCl_4$ from $HfCl_4$; (4) reduction of $ZrCl_4$ to a metallic Zr sponge; and (5) production of Zr metal with low Hf-contamination (less than 0.05 wt%) by Electron Beam Melting (EBM) or Vacuum Arc Remelting (VAR) both under high vacuum. Moreover, each step in this long production sequence can vary and can be adjusted aiming to optimise the chemical processes and the overall cost. Therefore, the list of the main chemical contaminants would vary for Zr metal samples of the same purity grade but purchased from different producers. Furthermore, even for Zr samples of the same producer but with different purity grades the list of contaminants might have drastic and unpredictable variations since the initial material will be taken at different stages of the Zr metal production chain for cost optimization. Thus, we decided to perform a comparative analysis of the two Zr metal samples obtained from different producers, following different chemical processes and final metal melting, focusing mostly on their radioactive contamination which is the only critical point when seeking rare nuclear processes in Zr isotopes.

Sample #1 was produced at Kharkiv Institute of Physics and Technology (KIPT, Ukraine) applying three-fold EBM under high vacuum [20]. The initial zirconium sponge was obtained through high-temperature decomposition of ZrI_4 (zirconium iodine) on a tungsten wire at 1300 °C. Then the Zr metal ingot was machined to obtain disks of 42 mm diameter and about 10 mm height (8 pcs) with a total mass of 736.35 g (see Fig. 2). The surface of all disks was etched by UP nitric acid, rinsed in UP water, and then dried under a high purity argon flux. As one can see from the data listed in Table 1, Zr metal produced in this way has a high chemical purity (99.9+% purity grade), containing Hf on the level of just 0.02 wt%. However, values for naturally radioactive elements such as potassium, thorium and uranium are typically not present in the datasheet, since they are not critical elements for Zr-alloy production used in industry. Thus, additional screening measurements are necessary.

Fig. 2 Sample #1, metallic zirconium disks produced by Electron Beam Melting (EBM) method

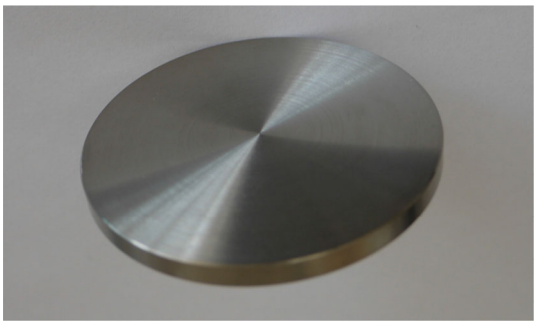

Fig. 3 Sample #2, metallic zirconium disk produced by Special Metals Fabrication Co. (Basildon, UK)

Sample #2 was produced by Special Metals Fabrication Co. (Basildon, UK). The Zr disk (Fig. 3) had 70.1 mm in diameter and was 5.18 mm thick, with a total mass of 129.94 g. The chemical purity of Zr Sample #2 was 98.1%, the admixture of Hf was 1.1 wt%.

3 Validation of the sample radiopurity

3.1 Chemical purity measurements

The chemical purity of Sample #1 was investigated using a high-resolution double-focusing laser mass spectrometry with an EMAL-2 (Mattauch–Herzog) spectrometer based on laser-plasma ion source. The results are reported in Table 2.

The chemical analysis of Sample #2 was carried out using the PIXE method [21]. Only detection limits (< 0.05 wt%) were obtained for Fe, Zn and Sn.

Table 2 Results of the laser mass spectrometry (Sample #1). Concentration values are given with a relative uncertainty of 30%

Element	wt%	Element	wt%
O	0.013	Fe	0.01
Cr	0.002	Hf	0.02
N	0.004	Al	0.003
Ti	0.0001	Ca	0.0001
C	0.025	Cu	0.0006
Si	0.005	F	0.0002
H	0.001	Ni	0.004
Nb	< 0.001	Mo	< 0.001

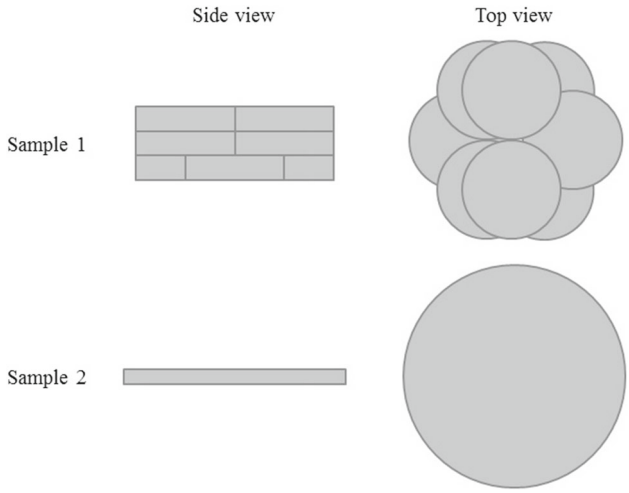

Fig. 4 Schematic view of zirconium Sample #1 and #2

3.2 Radiopurity measurements

The two zirconium samples were also measured via γ-spectrometry with ultra-low-background high-purity germanium detectors (ULB-HPGe). The measurements were carried out in the STELLA (SubTerranean Low-Level Assay) underground facility in Laboratori Nazionali del Gran Sasso (LNGS) [22–25].

Sample #1 was analyzed with a coaxial p-type germanium detector with an active volume of about 400 cm^3 and an energy resolution of 2.0 keV at 1332 keV line from ^{60}Co. To reduce the external background, the setup is shielded with a 20 cm layer of low-radioactivity lead, OFHC (Oxygen Free High Conductivity) copper ($\approx$ 5 cm), and a 5 cm layer of Polyethylene.

Sample #2 was measured on another coaxial p-type HPGe detector with a volume of 468 cm^3. The energy resolution of the spectrometer was 1.8 keV at 1332 keV line from ^{60}Co. It was also shielded by layers of low-radioactivity lead ($\approx$ 25 cm), copper ($\approx$ 5 cm), and ancient lead ($\approx$ 2 cm) on the inner part of the copper shield. To reduce radon, both detectors were continuously flushed with a boil-off nitrogen. The schematic views of the zirconium samples arrangement on the HPGe detectors are shown in Fig. 4. Data taking lasted 59.7 days for Sample #1 and 37.3 days for Sample #2, respectively. More details on both experimental setups and detector performance can be found in [26].

Table 3 Specific activities of naturally occurring radionuclides in the two zirconium metal samples measured by gamma-spectroscopy. Activity values are given in mBq/kg or Bq/kg. Upper detection limits are given with 90% CL

Chain	Nuclide	Activity		
		Sample 1	Sample 2	
^{238}U	^{234}Th	2.6 ± 0.6	33.8 ± 3.4	Bq/kg
	^{234m}Pa	2.3 ± 0.2	28.2 ± 2.8	Bq/kg
	^{226}Ra	< 1.1	< 3.2	mBq/kg
^{235}U	^{235}U	0.32 ± 0.04	1.34 ± 0.12	Bq/kg
	^{231}Pa	51.5 ± 3.7	14.7 ± 1.1	Bq/kg
	^{227}Ac	26 ± 1	2.88 ± 0.11	Bq/kg
^{232}Th	^{228}Ra	< 1.8	20 ± 3	mBq/kg
	^{228}Th	0.7 ± 0.3	19 ± 2	mBq/kg
	^{137}Cs	< 0.82	< 1.6	mBq/kg
	^{40}K	< 3.2	22 ± 7	mBq/kg

The list of radioactive nuclides found in the two zirconium samples is given in Table 3. These values were calculated using the procedure presented in [27]. The efficiencies for the full-energy peaks were determined using a Monte-Carlo simulation (MaGe code) based on the GEANT4 software package [28].

Comparing the results for the two zirconium samples in Table 3, one can see very different levels of radiopurity. Unfortunately, the purification efficiency that may occur during Zr metal melting cannot be determined since samples of the initial zirconium sponge were not measured.

4 Double beta decay of ^{94}Zr

Despite a low radiopurity of the zirconium metal samples in general, the acquired background spectra exhibit a reasonably low background counting rate around 870 keV allowing to perform a search for DBD of ^{94}Zr to excited states of ^{94}Mo. Due to a low energy release in ^{94}Zr DBD, only the first 2^+ state at 871.1 keV is accessible, therefore a single γ quantum of this energy is expected. Hence, in this analysis we perform a simultaneous Binned Extended Likelihood fit on the two data sets, taking into account all the background sources producing a peak in the energy range of the fit, [820–920] keV.

We assign a Gaussian $\mathcal{G}(\mu, \sigma)$ probability density function (p.d.f.) to each γ-line, assuming a constant energy res-

olution (σ) in the fit range for each detector. The continuous component is described with different models in the two data sets according to the different contaminations. In the energy spectrum collected with Sample #1, the multi-Compton contributions from ^{211}Pb and ^{207}Tl are evident and they add to a flat background. On the other hand, such contributions are negligible for Sample #2. Therefore, we decide to model the background in Sample #1 with a flat contribution (N_{flat}) plus the multi-Compton ones ($\mathcal{G}_{\text{compt}}$), while for Sample #2 an exponential p.d.f. ($e^{a\cdot E}$) is more appropriate.

In summary, the resulting p.d.f. are:

$$\mathcal{F}_1^{\beta\beta} = \sum_{i=1}^{3} N_i \cdot \mathcal{G}_{\text{compt}}(\mu_i, \sigma, f_i) + N_{\text{flat}} + S_1 \cdot \mathcal{G}(\mu, \sigma) \quad (3)$$

$$\mathcal{F}_2^{\beta\beta} = \sum_{i=1}^{7} N_i \cdot \mathcal{G}(\mu_i, \sigma) + N_{\text{exp}} \cdot e^{a\cdot E} + S_2 \cdot \mathcal{G}(\mu, \sigma) \quad (4)$$

where f determines the multi-Compton fraction as:

$$\mathcal{G}_{\text{compt}}(\mu, \sigma, f) = f\mathcal{G}(\mu, \sigma) + (1 - f)\,\text{Erf}\left(\frac{E-\mu}{\sqrt{2}\sigma}\right). \quad (5)$$

The signal is modelled as a Gaussian p.d.f. with the energy resolution constrained to be equal to the other peaks. The number of signal events is determined by:

$$S_i = \Gamma^{\beta\beta} \cdot \eta_i^{\beta\beta} \cdot N_i^{^{94}\text{Zr}}, \quad (6)$$

where $\Gamma^{\beta\beta}$ is the signal decay rate, $N^{^{94}\text{Zr}}$ is the number of Zr atoms, and $\eta^{\beta\beta}$ is the containment efficiency for a signal event. The efficiencies are evaluated with a simulation code and their values are $\eta_1^{\beta\beta} = 0.023 \pm 0.002$ and $\eta_2^{\beta\beta} = 0.062 \pm 0.003$.

The free parameters of the fit are: the resolution for each data set; the number of events for each distribution including background peaks (N_i) and flat (N_{flat}) contributions, the Gauss-Compton fraction f, the exponential (a) background coefficient, the energy resolution (σ), and the decay rate $\Gamma^{\beta\beta}$. From the best fit, reported in Fig. 5, the decay rate $\Gamma^{\beta\beta} = (-1.06 \pm 2.1) \times 10^{-21}$ year^{-1} is compatible with zero, thus no significant excess of events was found.

We perform a Bayesian analysis integrating the likelihood with a uniform prior and marginalizing over the nuisance parameters to set a limit on the half-life of $(0\nu + 2\nu)$DBD. This is done by exploiting the RooStat Bayesian Calculator tools. We treat as nuisance parameters the efficiencies, the number of events from the flat contributions, the systematic shifts, and the uncertainty on the exposures.

The resulting upper limit on the decay rate at 90% CI is $\Gamma^{\beta\beta} < 3.36 \times 10^{-21}$ year^{-1} (see Fig. 6), corresponding to a lower limit on the half-life,

$$T_{1/2}^{\beta\beta} > 2.1 \times 10^{20} \text{ year} \quad \text{at 90\% CI.} \quad (7)$$

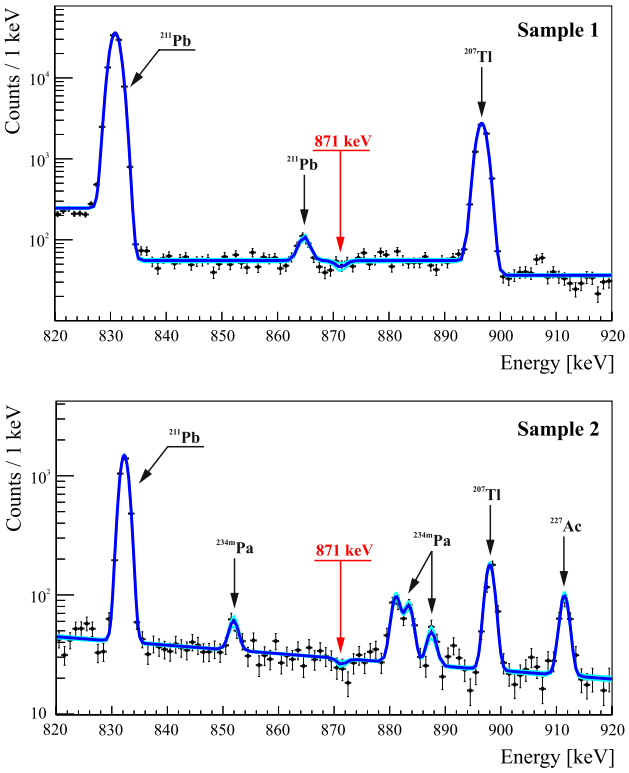

Fig. 5 Energy spectra of the acquired data. The first measurement (top) corresponds to 59.7 days of data taking with 736.35 g of natural zirconium, while the second one (bottom) corresponds to 37.3 days of data acquired with 129.94 g of natural zirconium. Black arrows and labels identify the γ peaks caused by radioactive contamination of the Zr samples included in the fit. The red arrow indicates the energy of the γ peak expected at 871 keV for the ^{94}Zr double beta decay to the first excited state of daughter nuclei. The dark blue line marks the best fit result, while the light blue lines report a $\pm 1\sigma$ statistical fluctuation of the number of counts of all the contributions

This result is almost a factor of four better than the previous limit on ^{94}Zr DBD half-life, equal to $T_{1/2} > 5.2 \times 10^{19}$ year at 90% CL [16].

At the same time, in this study we do not perform search for DBD of ^{96}Zr to excited states of ^{96}Mo, since the radiopurity of Zr metal samples and their geometry, as well as the used experimental setups are not optimized to improve the existing limits for this isotope. The current limits reported in Refs. [17,29], were obtained with a zirconium sample enriched in ^{96}Zr (up to 91.4%) and measured in coincidence with two HPGe detectors. This leads to a substantial background reduction with a subsequent enhancement of the experimental sensitivity.

5 Further developments

Since the sensitivity of our experiments is limited by the internal contamination of zirconium metal samples with radionu-

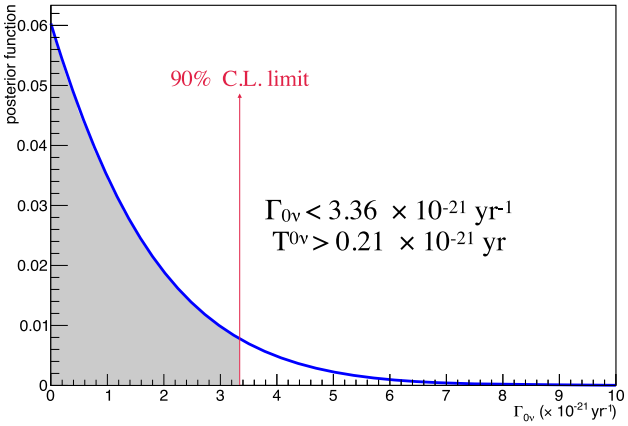

Fig. 6 Posterior distribution of the decay rate $\Gamma^{\beta\beta}$ obtained from the simultaneous fit of the two data sets

clides from Th and U decay chains, we decided to investigate a different Zr-containing compound that could be purified more effectively. Profiting from the promising results in $ZrCl_4$ powder purification for Cs_2ZrCl_6 crystal production, we decided to choose this Zr-containing material and purify it for our research purposes.

Anhydrous $ZrCl_4$ (99.9% purity grade, Sigma Aldrich), a white powder, was used as a starting material. It was purified using a two-stage sublimation process. In the first stage, 50 g of raw $ZrCl_4$ powder were loaded into a quartz ampule and sealed under high vacuum. Then the sealed ampule was placed into a horizontal furnace for sublimation at 380 °C over 24 h. After this stage, the $ZrCl_4$ powder now with a yellowish colour, was separated from non-volatile impurities of dark grey colour. At the second stage of purification, the $ZrCl_4$ was reloaded into a new quartz ampule, vacuum sealed and then underwent another sublimation step at a temperature of 300 °C. The final yield of the two-stage purification was 90% (45 g) [30].

The concentration of chemical impurities in the $ZrCl_4$ powder at the different stages of the purification process was determined via High Resolution Inductively Coupled Plasma Mass-Spectrometry analysis (HR-ICP-MS, Thermo Fisher Scientific ELEMENT2) at LNGS. The results are given in Table 4. The analysis was done in a semi-quantitative mode, calibrating the instrument with a single standard solution containing 10 ppb of Li, Y, Ce and Tl. The uncertainty is about 30% of the given concentration values. The $ZrCl_4$ samples were smashed to a fine powder in an agate mortar. Then, about 50 mg of each sample were placed in a plastic vial, filled with a 1 ml of nitric acid and placed in an ultrasonic bath at room temperature until full sample decomposition. The vials with the samples dissolved in this manner were prepared for a HR-ICP-MS analysis by adding ultra-pure water up to 10 ml of total volume, i.e. with a dilution factor of about 1000.

Table 4 Concentration of chemical impurities in the $ZrCl_4$ powder at different stages of the purification process, determined by a HR-ICP-MS analysis. The uncertainty is about 30% of the given concentration values expressed in ppb

Element	$ZrCl_4$ initial	$ZrCl_4$ 1st sublim.	$ZrCl_4$ 2nd sublim.
K	15,000	700	700
Hf	6400	5200	5600
Th	70	0.5	0.2
U	1000	7	0.4

Table 5 Specific activity of naturally occurring radionuclides in the purified $ZrCl_4$ powder sample measured by gamma-ray spectrometry. Activity values are given in mBq/kg or Bq/kg. Upper detection limits are given with 90% CL

Chain	Nuclide	Activity	
^{238}U	^{234}Th	< 0.2	Bq/kg
	^{234m}Pa	< 0.2	Bq/kg
	^{226}Ra	5 ± 2	mBq/kg
^{235}U	^{235}U	< 19	mBq/kg
	^{231}Pa	0.52 ± 0.06	Bq/kg
	^{227}Ac	18 ± 4	mBq/kg
^{232}Th	^{228}Ra	< 6	mBq/kg
	^{228}Th	< 6	mBq/kg
	^{137}Cs	< 0.3	mBq/kg
	^{40}K	< 67	mBq/kg

The results in Table 4 show that the initial $ZrCl_4$ sample is rather contaminated by potassium at the level of 15,000 ppb. This concentration was significantly reduced by the two-stage sublimation down to the level of about 700 ppb.

The purification is very efficient for the removal of U and Th. After the first stage, their concentration is reduced 140 times with respect to the initial concentration in the $ZrCl_4$ powder. After the second sublimation stage, their concentration is further reduced by a factor of 2.

A high concentration of Hf, determined in the initial $ZrCl_4$ powder (6400 ppb), was expected due to its chemical affinity with Zr. Hence, the sublimation reduces the Hf concentration only by a factor of 1.2. Therefore, a further improvement of this purification technique from Hf should be done either increasing the number of sublimation stages or adjusting the sublimation temperatures, or applying both together.

The radiopurity of the purified $ZrCl_4$ powder was measured with a ULB-HPGe detector in the STELLA facility at LNGS. The $ZrCl_4$ powder sample (45 g) was sealed in a polytetrafluoroethylene container that was placed directly on the end cup of the ULB-HPGe detector. Data have been acquired over 30 days. The results of this measurement are given in Table 5.

The results show a high radiopurity level of the Zr-containing compound, in two/three orders of magnitude better than for Zr metal samples, also with respect to the ^{235}U decay chain. In particular, the $ZrCl_4$ sample shows only upper detection limits for ^{232}Th and ^{235}U/^{238}U, well in agreement with the HR-ICP-MS results, that could be explained by a highly efficient purification process for these elements. Furthermore, one can clearly see that the secular equilibrium in the ^{238}U decay chain is broken at ^{226}Ra, whereas in the ^{235}U chain it is broken at ^{231}Pa and ^{227}Ac. However, even relatively high activities of the latter two radionuclides and their progeny are not relevant for DBD searches to excited states in Zr isotopes, since they emit gammas with relatively low energies (below 840 keV), thus well below the regions of interest for DBD signal of ^{94}Zr.

The upper detection limit for ^{40}K, less than 67 mBq/kg, is corresponding to a concentration of natural potassium of less than 2 ppm. This value is in a perfect agreement with the actual concentration of potassium measured with HR-ICP-MS (0.7 ppm).

Based on these achievements in chemical and radio-purity of the Zr-containing compound, the next step will be to purify a few kilograms of $ZrCl_4$, fill it into a vacuum-sealed container in an optimized geometry (e.g. a Marinelli container), and perform a long-term measurement, aiming for a 10^{22} (10^{21}) year sensitivity for the half-lives of rare processes occurring in natural ^{94}Zr (^{96}Zr) isotopes, respectively.

6 Conclusions

In the this study, the most stringent limit on DBD of ^{94}Zr to the excited level of its daughter nuclide ^{94}Mo was set at the level of $T^{\beta\beta}_{1/2} > 2.1 \times 10^{20}$ year, combining two sets of measurements with two different Zr metal samples. While this limit cannot be competitive to tonne-scale DBD-experiments, it is a useful bench-top measurement to extend the list of isotopes under investigation for theoretical modelling.

As shown above, Zr metal and Zr-containing compound samples although having similar chemical purity show a very different elemental composition of their internal impurities. This depends, most probably, on the starting material origin and on the used production procedure. The Zr metal of a high internal radiopurity can be obtained only on a laboratory scale production, where one can control all technological steps, the purity of the utilized reagents and labware. The stringent radiopurity requirements of low-background experiments for chemicals, equipment and handling protocols cannot be satisfied on an industrial production scale, since radiopurity of Zr metal and its alloys is not considered critical for industrial applications.

It was also shown that the multi-fold vacuum distillation of the $ZrCl_4$ powder is a very effective purification method for reducing the concentration of ^{40}K and radionuclides from U/Th decay chains. Hence, it seems to be more attractive to focus efforts on the $ZrCl_4$ powder purification instead of Zr metal, which would require additional steps to transform the initial metal into the appropriate chemical compound.

One common approach to increase the number of decaying nuclei is to use enriched material, see for instance [31]. However, this becomes difficult for Zr isotopes as they can only be enriched by Electro-Magnetic Separation, a very expensive and time-consuming process. Price estimates give a value of about \$500/mg for 90% enrichment. With adequate funding, one could increase the sensitivity by a factor of 30. Further improvement of the experimental sensitivity can be achieved through the reduction of the sample dimensions, thus enhancing the detection efficiency by reducing the self-absorption for de-excitation gammas in the sample. Another complication is associated with the limited worldwide available quantity of enriched ^{94}Zr and ^{96}Zr isotopes ($\sim$ few tens of grams). Therefore, an alternative way to investigate rare decays in natural Zr to excited states of daughter nuclei with enhanced sensitivity is the combination of ULB HPGe detectors with a large mass of purified Zr-containing compounds in an optimized sample geometry to maximize the detection efficiency.

An alternative method to this could be using the "source = detector" experimental approach, where Zr is embedded directly inside the detector material, e.g. Cs_2ZrCl_6 crystals with a Zr-content of 16% and excellent scintillation properties [30,32].

Data Availability Statement This manuscript has no associated data or the data will not be deposited. [Authors' comment: Data will be made available on reasonable request to the corresponding author.]

Funded by SCOAP^3. SCOAP^3 supports the goals of the International Year of Basic Sciences for Sustainable Development.

References

1. F. Vissani, Universe **7**(3), 61 (2021). https://doi.org/10.3390/universe7030061

2. A.S. Barabash et al., Phys. Rev. D **98**(9), 092007 (2018). https://doi.org/10.1103/PhysRevD.98.092007
3. S. Abe et al. Phys. Rev. Lett. **130**(5), 051801 (2023). arXiv:2203.02139
4. M. Agostini et al., Phys. Rev. Lett. **125**(25), 252502 (2020). https://doi.org/10.1103/PhysRevLett.125.252502
5. I.J. Arnquist et al., Phys. Rev. Lett. **130**(6), 062501 (2023). https://doi.org/10.1103/PhysRevLett.130.062501
6. D.Q. Adams et al., Nature **604**(7904), 53 (2022). https://doi.org/10.1038/s41586-022-04497-4
7. O. Azzolini et al., Phys. Rev. Lett. **129**(11), 111801 (2022). https://doi.org/10.1103/PhysRevLett.129.111801
8. C. Augier et al., Eur. Phys. J. C **82**(11), 1033 (2022). https://doi.org/10.1140/epjc/s10052-022-10942-5
9. V. Alenkov et al., Eur. Phys. J. C **79**(9), 791 (2019). https://doi.org/10.1140/epjc/s10052-019-7279-1
10. G. Anton et al., Phys. Rev. Lett. **123**(16), 161802 (2019). https://doi.org/10.1103/PhysRevLett.123.161802
11. E. Aprile et al., Nature **568**(7753), 532 (2019). https://doi.org/10.1038/s41586-019-1124-4
12. Y. Fukuda, S. Moriyama, K. Hiraide, I. Ogawa, T. Gunji, R. Hayami, S. Tsukadaw, S. Kurosawa, J. Phys. Conf. Ser. **1468**(1), 012139 (2020). https://doi.org/10.1088/1742-6596/1468/1/012139
13. J. Argyriades et al., Nucl. Phys. A **847**, 168 (2010). https://doi.org/10.1016/j.nuclphysa.2010.07.009
14. M. Alanssari et al., Phys. Rev. Lett. **116**(7), 072501 (2016). https://doi.org/10.1103/PhysRevLett.116.072501
15. K. Gulyuz et al., Phys. Rev. C **91**(5), 055501 (2015). https://doi.org/10.1103/PhysRevC.91.055501
16. N. Dokania, D. Degering, B. Lehnert, V. Nanal, K. Zuber, J. Phys. G **45**(7), 075104 (2018). https://doi.org/10.1088/1361-6471/aac7ed
17. S.W. Finch, W. Tornow, Phys. Rev. C **92**(4), 045501 (2015). https://doi.org/10.1103/PhysRevC.92.045501
18. B. Broerman, M. Laubenstein, S. Nagorny, N. Song, A.C. Vincent, Nucl. Phys. A **1012**, 122212 (2021). https://doi.org/10.1016/j.nuclphysa.2021.122212
19. M.M. Pylypenko et al., PAST Ser.: Phys. Radiat. Damage Radiat. Mater. Sci. **2**, 66 (2008)
20. V.M. Azhazha et al., PAST Ser.: Phys. Radiat. Damage Radiat. Mater. Sci. **6**, 95 (2002)
21. J. Zeman, M. Ješkovský, J. Kaizer, J. Pánik, I. Kontul', J. Staníček, P. Povinec, J. Radioanal. Nucl. Chem. **322**(2), 1897 (2019). https://doi.org/10.1007/s10967-019-06851-9
22. C. Arpesella, Appl. Radiat. Isot. **47**(9), 991 (1996). https://doi.org/10.1016/S0969-8043(96)00097-8
23. H. Neder, G. Heusser, M. Laubenstein, Appl. Radiat. Isot. **53**(1), 191 (2000). https://doi.org/10.1016/S0969-8043(00)00132-9
24. G. Heusser, M. Laubenstein, H. Neder, in *Radionuclides in the Environment, Radioactivity in the Environment*, vol. 8, ed. by P. Povinec, J. Sanchez-Cabeza (Elsevier, Amsterdam, 2006), pp. 495–510. https://doi.org/10.1016/S1569-4860(05)08039-3
25. D. Budjas et al. (2008). arXiv:0812.0768
26. M. Laubenstein, Int. J. Mod. Phys. A **32**(30), 1743002 (2017). https://doi.org/10.1142/S0217751X17430023
27. M. Heisel, F. Kaether, H. Simgen, Appl. Radiat. Isot. **67**(5), 741 (2009). https://doi.org/10.1016/j.apradiso.2009.01.028. 5th International Conference on Radionuclide Metrology-Low-Level Radioactivity Measurement Techniques ICRM-LLRMT'08
28. M. Boswell et al., IEEE Trans. Nucl. Sci. **58**(3), 1212 (2011). https://doi.org/10.1109/TNS.2011.2144619
29. S. Finch, W. Tornow, Nucl. Instrum. Methods A **806**, 70 (2016). https://doi.org/10.1016/j.nima.2015.09.098
30. V. Mykhaylyk, S.S. Nagorny, V.V. Nahorna, P. Wang, M.D. Frogley, L. Swiderski, V. Kolomiets, L. Vasylechko, Dalton Trans. **51**, 6944 (2022). https://doi.org/10.1039/D2DT00223J
31. A. Armatol et al. (2022). arXiv:2203.08386
32. S. Nagorny, Physics **3**(2), 320 (2021). https://doi.org/10.3390/physics3020023